Material and Geometric Effects on Mass Reduction and Structural Performance of an Implicitly Morphed Lattice

Faisal Abdul Qader
Independent Researcher [Hyderabad, India]; ORCID: 0009-0004-9754-1918
Email: faisalabdulqader35@gmail.com

Abstract

Energy Storage and Return (ESAR) prosthetic blades are designed to meet design objectives of low mass, sufficient structural margin under physiological loading, and manufacturability. This study presents a staged engineering analysis of a prosthetic geometry, structured across four phases to study and analyze the effects of material selection, lattice geometry, and a structural workaround on mass and performance. Starting from an openly available prosthetic-leg geometry, the blade was evaluated as (Phase 1) a solid AISI 304 stainless steel baseline, (Phase 2) a solid composite baseline using the same geometry and load case, (Phase 3) a graded lattice design combining a hexagonal-truss zone, a body-centered-cubic (BCC) zone, and a field-driven transition zone, and (Phase 4) a homogenized-property structural evaluation of that lattice design using Gibson-Ashby cellular-solid scaling. A 700 N physiological load, derived from a 70 kg nominal body mass, was applied as a pressure boundary condition, with an independently calculated contact area and pressure for the heel (2457 mm², 0.285 MPa) and the toe (4432.9 mm², 0.157 MPa), and the shin-cup interface fixed as the structural constraint. The steel baseline failed under this load (Factor of Safety, FOS, of 0.2 at the heel and 0.3 at the toe), while the composite baseline survived at both locations (FOS 1.6 at the heel and 2.5 at the toe), isolating a clear material effect. Because direct explicit finite-element simulation of the sub-millimeter lattice strut geometry could not be resolved by the meshless solver used in this study, each lattice zone was instead assigned a homogenized material property card, derived by scaling the parent composite's stiffness, density, and yield strength using Gibson-Ashby relationships at the design's relative density, and this homogenized-property body was then structurally analyzed directly. This workaround identified a structurally inadequate lattice region near the shin-cup interface (FOS below 1), which was corrected back to solid material before the final configuration was reported. The final homogenized lattice design achieved a mass of 0.171 kg against the 0.968 kg steel baseline, an overall reduction of approximately 82.3%, of which the majority is attributable to material substitution and a smaller share to lattice geometry and the subsequent cup-region correction. The final lattice configuration returned a minimum FOS of 1.1 at the heel and 2.0 at the toe under the homogenized-property approximation. These results support treating material selection and lattice geometry as separable, additive contributors to mass reduction, and demonstrate a practical, literature-consistent workaround for approximating lattice structural performance when direct strut-level simulation is not feasible.

Keywords: ESAR prosthetic blade; lattice structure; Gibson-Ashby scaling; homogenized material properties; carbon-fiber composite; finite element analysis; mass reduction; relative density

1. Introduction

The ESAR prosthesis for feet comes in the form of artificial feet and blades that have a dynamic response during usage; they store energy and release it in turn, mimicking a leg when used. These are passive elastic structures that are designed to store energy during the loading phase of the walking pattern of the person, and return this energy during takeoff of the feet, in turn mimicking the biomechanical function. The structural function approximates the spring-like behavior of the Achilles tendon and the foot arch. The structural performance of an ESAR prosthesis is jointly governed by the geometry & design, the material that is used for its manufacturing and the internal build or the architecture of the design as well. Reducing the blade mass while conserving its structural performance and functionality is essential. From one perspective, this would enhance the user's comfort. But on the other perspective, the mass reduction might compromise structural margin under physiological loading.

This study addresses a design question that is common in light weighting methodology. The question that persist even after a part is both re-material and lattice-optimized; What change would attribute to changing material in terms of performance and reduction of mass, would it be due to the mass reduction only or due to the resulting geometry as well. This work isolates these resulting effects using a four-phase methodology applied to a single, fixed blade geometry. The material effect being studied in the Phase 1 vs Phase 2 comparison, the lattice geometry effect in the Phase 2 vs Phase 3 comparison and finally the structural consequence of that lattice geometry studied in the Phase 4, these are done to avoid everything to be in a single confounded design change.

Simulating lattice geometries at the individual strut level is often computationally difficult, due to their fine and complex features, especially when using standard or meshless solvers. Rather than avoiding this challenge, this problem was addressed in Phase 4 by introducing a homogenized-property analytical method based on the Gibson-Ashby cellular solid theory. This approach gives an approximation of the lattice behavior when resolving the geometry is unfeasible.

2. Methodology

2.1 Source Geometry and Model Preparation

The blade geometry (250 mm length, 55 mm width, 3 mm single-layer thickness stepping to 6 mm at the doubled toe section) was derived from the open-source GrabCAD prosthetic leg model referenced (Nox, 2017). The assembly was downloaded, cleaned, and reassembled in SolidWorks, with the shin-cup mounting interface retained throughout all four phases as a fixed constraint. While the mounting cup and bracket interface which is basically the thing that is surrounding all the lattice sites, were preserved as solid material in every phase, ensuring the load-introduction and constraint regions remained geometrically and structurally consistent throughout the study.

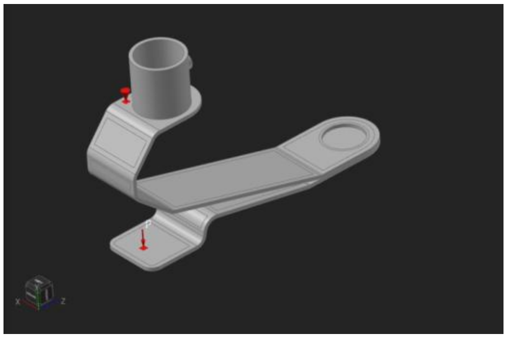

Figure 1. Solid baseline blade geometry (mass = 0.968 kg, AISI 304 steel) with applied pressure load (P) at the toe contact region and fixed support at the shin-cup interface.

2.2 Simulation Approach through SimSolid Meshless Analysis

Structural analysis in this study was performed using SimSolid, run within Altair Inspire. SimSolid uses a fundamentally different numerical approach from conventional finite element analysis (FEA). Traditional FEA requires the geometry to first be broken down into a fine mesh of small elements, before the underlying equations can be solved; generating a good-quality mesh, especially for complex or thin-walled geometry, is often the most time-consuming and susceptible to error in this analysis process, and a poorly-formed mesh can produce inaccurate results or cause the solver to fail entirely. SimSolid uses a meshless (mesh-free) method which works directly on the original, unmeshed CAD geometry, using a proprietary system of approximating functions to represent how the structure deforms under load, refining the accuracy of the solution locally and automatically in regions of interest, without the user needing to manually mesh the part. By bypassing traditional mesh generation, this method enables fast, direct analysis of complex, thin-walled, or multi-part geometries. This meshless approach was well suited to the solid-body phases of this study (Phases 1 and 2), and, as described in Section 2.9, also enabled the homogenized-property lattice analysis of Phase 4; it did not, however, resolve the literal strut-level lattice geometry produced in Phase 3, which motivated the homogenization workaround.

2.3 Load Case and Pressure Calculation

The body weight of a typical adult wearer would be about 70 kg, and a load for a typical single-limb stance with this average body mass and the corresponding body-weight force is calculated as follows.

$$\mathbf{F = m \times g = 70\ kg \times 9.81\ m/s^2 \approx 686.7\ N \approx 700\ N}$$

where m is the assumed body mass and g is standard gravitational acceleration. This 700 N value was held constant across every structurally-analyzed phase of this study, so that the load itself never changes; only the material, and later the geometry, changes between phases, allowing the comparative results in Section 3 to be attributed to material or geometric effects instead to differences in loading.

Rather than applying this force as a single point load, which would create an artificial and unrealistic stress concentration, the force was converted into a pressure and distributed over the physical contact area through which a wearer's weight is actually transmitted into the blade. Pressure is simply force divided by the area over which that force acts:

$$P = F / A$$

For the heel contact region, the contact area was measured directly from the geometry as approximately 2457 mm², giving:

$$P(\text{heel}) = 700\ \text{N} / 2457\ \text{mm}^2 \approx 0.285\ \text{MPa}$$

Since the toe region is bounded by circular ring geometry that is harder to measure precisely. This assumption was with an independently measured toe contact area of approximately 4432.9 mm², giving a toe pressure of:

$$P(\text{toe}) = 700\ \text{N} / 4432.9\ \text{mm}^2 \approx 0.157\ \text{MPa}$$

Heel-loading and toe-loading were run as separate linear static load cases at each phase, since a wearer loads these two regions at different phases of gait, and the governing (more critical) location was not assumed in advance.

2.4 Material Properties

Two base materials were used across the comparative phases:

- AISI 304 austenitic stainless steel — standard material library properties were used (typical published values: elastic modulus ≈ 193 GPa, yield strength ≈ 215 MPa, density ≈ 8000 kg/m³), representing a conventional, non-optimized prosthetic blade material baseline.
- Carbon-fiber-representative composite (“ESAR prosthetic material,” custom material definition) — elastic modulus $E = 1.5 \times 10^5$ MPa, Poisson's ratio $\nu = 0.3$, density $\rho = 1.6 \times 10^{-6}$ kg/mm³ (1600 kg/m³), yield strength $= 1.8 \times 10^3$ MPa, defined to represent a high-performance carbon-fiber-composite blade material consistent with commercial ESAR blade construction, acknowledged as a representative engineering approximation rather than a layup-specific, experimentally measured.

Property	Symbol	Value
Elastic modulus	E	1.5×10^5 MPa
Poisson's ratio	ν	0.300
Density	ρ	1.6×10^{-6} kg/mm³ (1600 kg/m³)
Yield stress	—	1.8×10^3 MPa
Thermal expansion coefficient	α	5.0×10^{-7} /K
Thermal conductivity	λ	1.620×10^{-2} W/(mm·K)
Specific heat	C_p	9.000×10^2 J/(kg·K)

Table 1. Custom composite material property definition (“ESAR prosthetic material”) used as the parent material for Phase 2 and as the basis for the homogenized lattice-zone material cards in Phase 4.

2.5 Phase 1 — Solid AISI 304 Steel Baseline

The full blade geometry was analyzed as a solid AISI 304 part under the load cases defined in Section 2.3, in essence with respect to heel and the toe, to establish a conventional-material baseline for both mass and structural performance. This was also done in order to set a baseline comparison metric for the composite mass and later for the mass of the lattice construction in various sites of the design as well.

2.6 Phase 2 — Solid ESAR Composite Baseline

The identical blade geometry and load case from Phase 1 was re-analyzed with the material changed to the custom composite definition Table 1, with no other changes to geometry, mesh strategy, load, or constraints. This isolates the effect of material substitution alone on both mass and structural response.

2.7 Phase 3 — Lattice Site Introduction

With the composite material established as the structurally viable baseline, a localized site based lattice architecture was then introduced into the design, following an implicit part creation workflow in Altair Inspire in which the design-space that was planned to be dedicatedly lattice-filled, based on type of loads on the area of the design, in essence the heel and the toe region divided into zones and the bridge being the transition zone. The choice of lattice topology in each zone was based on the differing mechanical demands anticipated across the blade:

- Zone A (heel region, extending through the shin-cup mount): a hexagonal-truss (hex-truss) unit cell: 3mm cell size, strut diameter: 0.6 mm, was selected for its characteristics being in bending compliance, which is favorable for energy absorption during the heel-strike phase of gait. (Hössinger-Kalteis, et al., 2024)
- Zone B (toe region and underside): a body-centered-cubic (BCC) unit cell: 2 mm cell size, strut diameter: 0.7 mm, was) selected for its stretch-dominated load path, which favors efficient, direct force transmission during the toe-off phase of gait, where the stored energy is returned and load is carried more directly through the structure. (Alwattar & Mian, 2020)
- Transition zone (≈ 20% of blade length, centered toe-ward of the blade midpoint): a field-driven spatial morph along the local build/thickness axis, blending Zone A and Zone B topologies to avoid a stress-concentrating interface between the two lattice types.

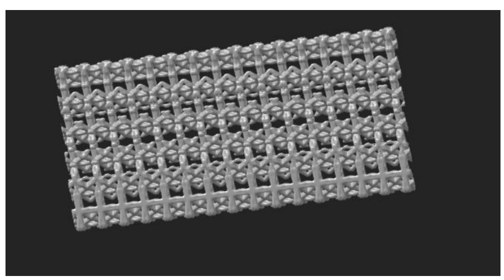

(Jalali, Beigrezaee , Misseroni, & Pugno , 2024)

Figure 2. Zone A — hexagonal-truss lattice detail (3 mm cell, 0.6 mm strut).

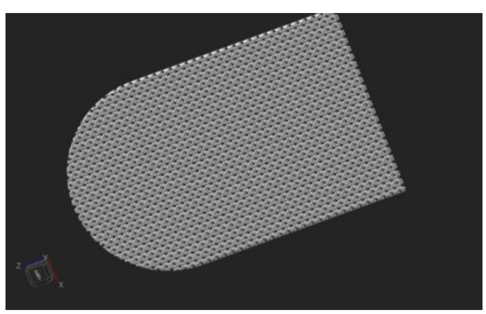

Figure 3. Zone B — body-centered-cubic (BCC) lattice detail (2 mm cell, 0.7 mm strut).

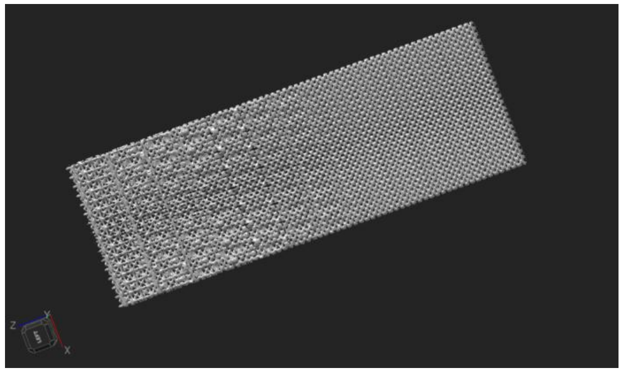

Figure 4. Transition zone showing the field-driven hex-truss → BCC morph (≈ 20% of blade length).

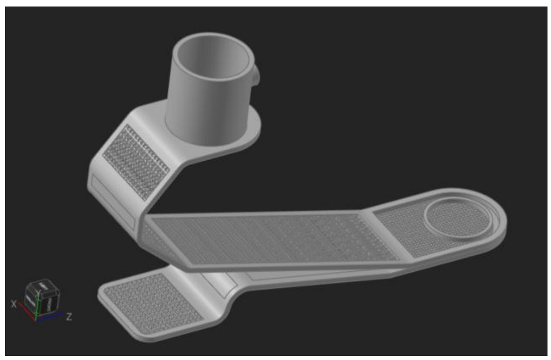

Figure 5. Initial composite graded-lattice geometry and recorded mass (0.14 kg), prior to the Phase 4 cup-region correction.

The AISI 304 material had its weight as 0.968 kg, when a localized lattice structure was introduced the weight was reduced to 0.698 kg. Now when the composite material was introduced for the overall body, the mass reduction lessened even more to 0.194 kg, when the lattice structures were introduced to this model with the composite mass, the mass lessened even more to 0.14 kg. This approach was to solely test whether the geometric mass-reduction produced by a given lattice pattern depends on the base material or the geometry alone.

2.8 Understanding Lattice Stiffness Behavior — Gibson-Ashby Cellular Solid Scaling

At this point in the design process, applying the lattice geometry from Section 2.7 directly into the SimSolid solver did not produce usable structural results (refer Section 2.9 for a full explanation). Before describing the workaround adopted, it is useful to explain what Gibson-Ashby scaling is and why it is relevant here. Any lattice or foam-like structure is, mechanically, a solid material with material removed from it in a repeating pattern. Removing material makes the structure lighter, but it also makes it less stiff. A block of material with lots of small holes cut out of it will bend more easily under the same load than the same block left solid. The Gibson-Ashby framework, developed in the field of cellular solids mechanics, provides a mathematical way to estimate how much stiffness is lost for a given amount of material removed, without needing to simulate the exact lattice geometry strut-by-strut. (Jalali, Beigrezaee , Misseroni, & Pugno , 2024).

The key input to this framework is relative density. The ratio of the lattice's mass (or volume) to the mass (or volume) of the same shape if it were fully solid. A relative density of 100% means solid material; a relative density of, for example, 72% means 28% of the material has been removed to form the lattice. Gibson-Ashby theory shows that the relationship between relative density and stiffness is not a simple straight line — it also depends on how the lattice's internal struts carry load. In stretch-dominated lattices, the struts are arranged so that most of them are pulled or pushed along their length (stretched or compressed) under load, which is a mechanically efficient way to carry force, and stiffness drops off roughly in direct proportion to relative density. In bending-dominated lattices, the struts are arranged so that many of them bend sideways under load, which is mechanically less efficient, and stiffness drops off much faster, approximately with the square of relative density, as material is removed. This distinction is important for this study because the two lattice zones used here (Section 2.7) are not the same type: the BCC unit cell used in Zone B is stretch-dominated, while the hex-truss unit cell used in Zone A is bending-dominated, so the two zones would not be expected to lose stiffness at the same rate even at an identical relative density. The specific scaling relationship used in this study, for a lattice of relative density $\rho^*/\rho s$, is:

$$\mathbf{E^* / Es \approx (\rho^*/\rho s)^n}$$

where $n \approx 1$ for stretch-dominated topologies (Zone B, BCC) and $n \approx 2$ for bending-dominated topologies (Zone A, hex-truss). In the following section, this relationship is used not merely as a theoretical expectation, but as the direct basis for constructing homogenized material property cards that were then used to obtain real, solver-based structural results for the lattice zones. (Meyer, Brenne, Niendorf, & Mittelstedt, 2020).

2.9 Homogenized Material Card Construction and Structural Analysis (Phase 4)

Resolving sub-millimeter strut features (0.6–0.7 mm) across a multi-zone graded lattice requires extremely fine local discretization, and converting the implicit lattice geometry into an explicit, contact-ready solid for analysis introduced boolean and connector errors that prevented the solver from evaluating the strut geometry. Rather than leaving the lattice zones without any structural evaluation, this study adopted an established workaround from cellular-solids engineering. By representing each lattice zone not as its literal strut geometry, but as a solid region with effective & homogenized material properties, scaled down from the parent composite material using the Gibson-Ashby relationships introduced in Section 2.8, at the design's measured relative density of approximately 72%. This is an approximate, average-behavior representation of the lattice, not a substitute for strut-level simulation; to achieve a structurally meaningful comparison.

The homogenized properties for each zone were calculated as follows. For the elastic modulus, the Gibson-Ashby relationship from Section 2.8 was applied using the relative density value of 0.72 and the appropriate exponent for each zone's dominant strut behavior:

- Zone A (hex-truss, bending-dominated, $n = 2$):

$$\mathbf{E^* = 1.5 \times 10^5\ MPa \times (0.72)^2 = 1.5 \times 10^5 \times 0.5184 \approx 7.776 \times 10^4\ MPa}$$

- Zone B (BCC, stretch-dominated, n = 1): (Meyer, Brenne, Niendorf, & Mittelstedt, 2020)

$$\mathbf{E^* = 1.5 \times 10^5\ MPa \times (0.72)^1 = 1.5 \times 10^5 \times 0.72 = 1.080 \times 10^5\ MPa}$$

- Transition zone: assigned the simple average of the Zone A and Zone B moduli,

$$\mathbf{(7.776 \times 10^4 + 1.080 \times 10^5) / 2 \approx 9.288 \times 10^4\ MPa}$$

representing the blended hex-truss/BCC behavior of this region.

Density was scaled linearly with relative density for all three zones, consistent with the definition of relative density itself: $\rho^* = 1.6 \times 10^{-6}$ kg/mm³ $\times$ 0.72 $\approx 1.152 \times 10^{-6}$ kg/mm³. Yield stress was scaled linearly for all three zones as a simplifying assumption (a single scaling rule applied uniformly, rather than a topology-dependent yield relationship): $\sigma_y^* = 1.8 \times 10^3$ MPa $\times$ 0.72 $\approx 1.296 \times 10^3$ MPa. This is a simplification worth noting explicitly: unlike stiffness, yield behavior in cellular solids is also known in the literature to depend on strut topology, and a single linear scaling rule was used here for tractability rather than topology-specific yield scaling. (Greer & Deshpande , 2019)

Material	E (MPa)	ν	Density (kg/mm³)	Yield (MPa)
ESAR prosthetic material (parent)	1.500×10^5	0.300	1.600×10^{-6}	1.800×10^3
Zone A (hex-truss, bending-dominated, n=2)	7.776×10^4	0.300	1.152×10^{-6}	1.296×10^3
Zone B (BCC, stretch-dominated, n=1)	1.080×10^5	0.300	1.152×10^{-6}	1.296×10^3
Transition zone	9.288×10^4	0.300	1.152×10^{-6}	1.296×10^3

Table 2. Homogenized material property cards for each lattice zone, derived from the parent composite material (Table 1) using Gibson-Ashby scaling at a relative density of 0.72.

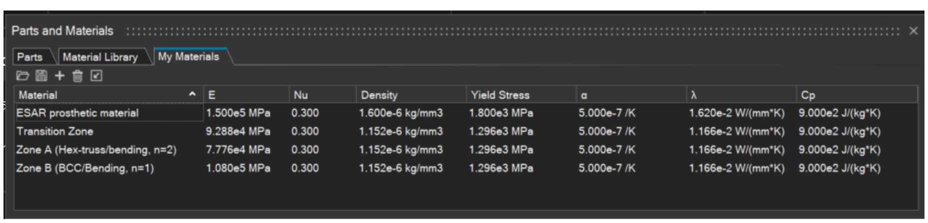

Figure 6. Material card definitions in Altair Inspire for the parent composite, transition zone, Zone A, and Zone B, corresponding to Table 1 and Table 2.

These homogenized material cards were then assigned directly to their respective solid zone bodies in place of the explicit lattice geometry, producing a structurally analyzable body that approximates the lattice's expected average mechanical behavior at its target relative density, without requiring the solver to resolve individual struts. During initial setup, Inspire's automatically-generated connectors between the separate zone bodies produced errors and did not reliably transmit load across zone boundaries. These automatic connectors were deleted, and contact-based connections were instead defined manually between the relevant bodies using the Contact feature under the Connections tab in the Structure module. This manual contact definition resolved the boundary-transmission errors and allowed the analysis to run successfully, producing displacement, von Mises stress, and Factor of Safety results for the homogenized lattice-zone configuration, presented in Section 3.4.

Running this homogenized-property analysis served a second, practical purpose beyond providing headline results: it was used to check the structural adequacy of the initial lattice design itself. The initial design (Section 2.7) included a lattice region on the inclined section near the shin-cup interface; the homogenized-property analysis showed this region returning a Factor of Safety below 1, indicating inadequate structural margin. This region was consequently reverted to solid material, and it is this corrected configuration that is reported as the final Phase 4 design and result in Section 3.4. This sequence, using an approximate structural evaluation method to catch and correct a design weakness before finalizing the geometry, is presented in this study as a demonstration of the practical value of the homogenization workaround, not only as a way of estimating headline performance.

At this stage, the lattice design also included a lattice region on the inclined section of the blade near the shin-cup interface. As reported in Section 3.3, this region was later found to be structurally inadequate once a structural evaluation became possible (Phase 4), and was reverted to solid material; the geometry and mass reported in this section (Section 2.7 and Section 3.3) reflect the initial lattice design, prior to that correction.

3. Results

3.1 Phase 1(Solid AISI 304 Steel Baseline)

The solid steel baseline recorded a mass of 0.968 kg. Under the 700 N pressure-load case, both the heel and toe loading conditions produced a Factor of Safety below 1, indicating structural failure at both locations.

Load Case	Pressure (MPa)	Displacement (mm)	Von Mises Stress (MPa)	FOS (min)
Heel	0.285	63.15	1153	0.2
Toe	0.157	61.55	715.2	0.3

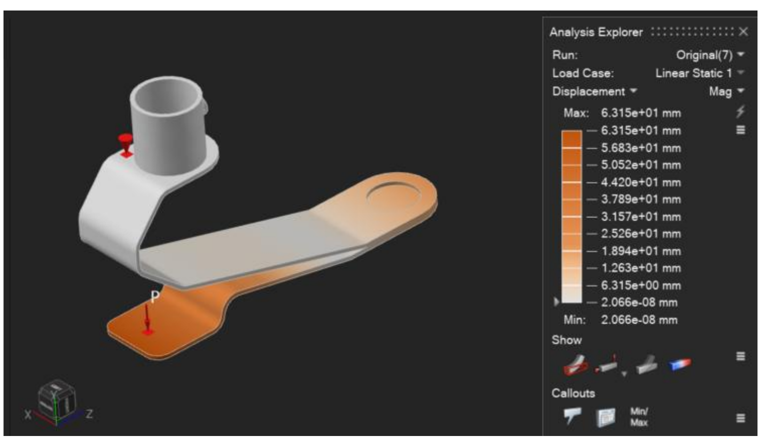

Figure 7. Phase 1 (steel) heel-loading displacement contour, max 63.15 mm.

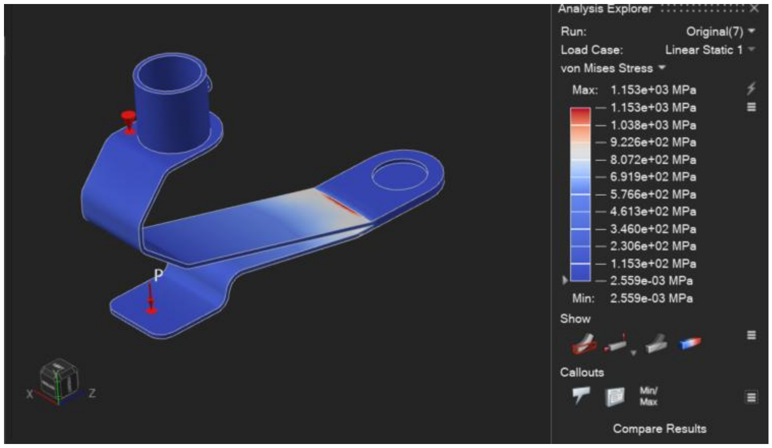

Figure 8. Phase 1 (steel) heel-loading von Mises stress contour, max 1153 MPa.

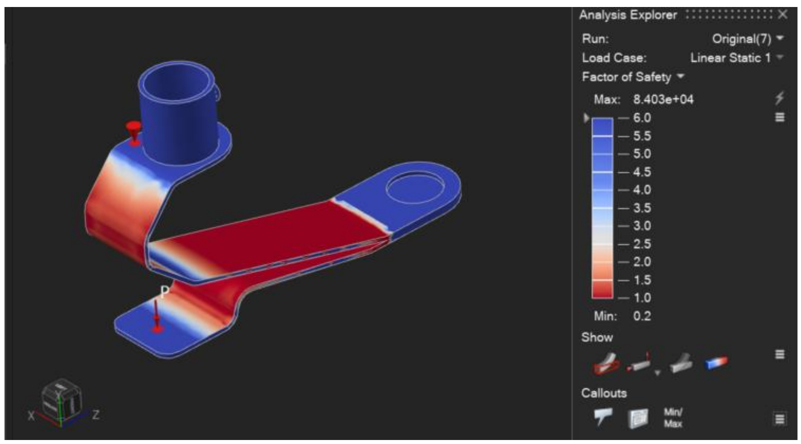

Figure 9. Phase 1 (steel) heel-loading Factor of Safety contour, min 0.2.

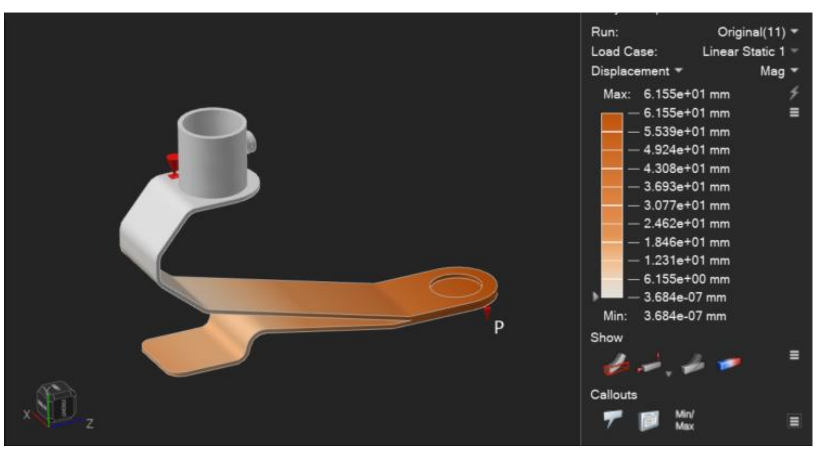

Figure 10. Phase 1 (steel) toe-loading displacement contour at the corrected 0.157 MPa pressure, max 61.55 mm.

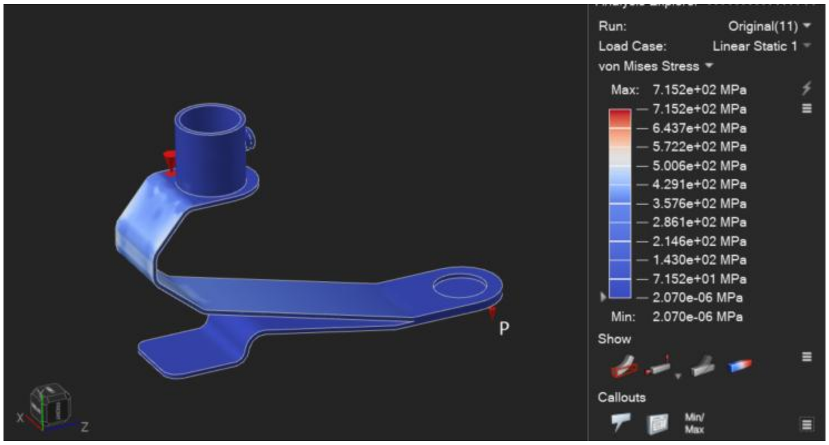

Figure 11. Phase 1 (steel) toe-loading von Mises stress contour at the corrected 0.157 MPa pressure, max 715.2 MPa.

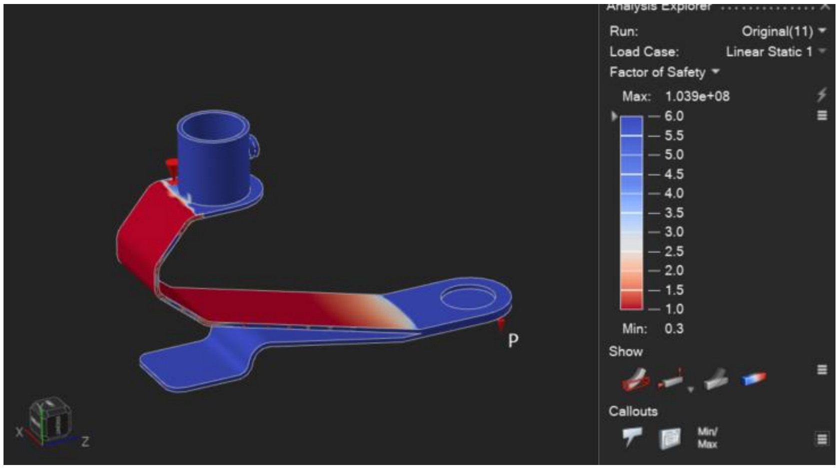

Figure 12. Phase 1 (steel) toe-loading Factor of Safety contour at the corrected 0.157 MPa pressure, min 0.3.

At this corrected toe pressure, the heel location is the more structurally critical of the two for the steel baseline (FOS 0.2 vs. 0.3), though both fail well below the required safety margin.

3.2 Phase 2 (Solid ESAR Composite Baseline)

With the material changed to the composite (Section 2.4) and all other things held constant, the solid mass reduced to 0.194 kg. Under the identical load case, both heel and toe locations maintained a Factor of Safety above 1, indicating the part survives the applied physiological load at this phase.

Load Case	Pressure (MPa)	Displacement (mm)	Von Mises Stress (MPa)	FOS (min)
Heel	0.285	81.92	1156	1.6
Toe	0.157	79.76	714.1	2.5

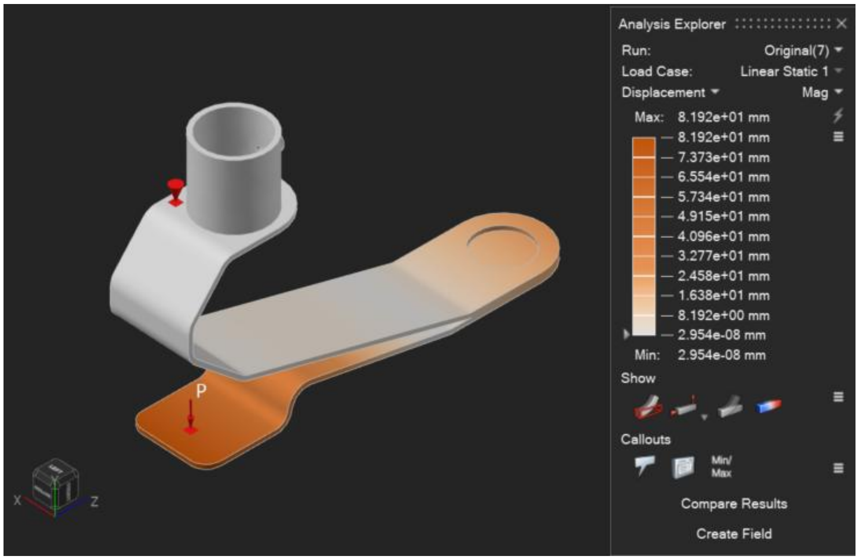

Figure 13. Phase 2 (composite) heel-loading displacement contour, max 81.92 mm.

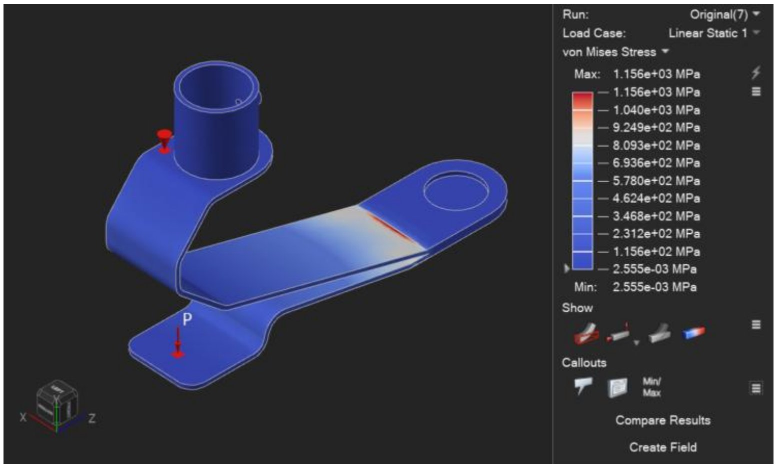

Figure 14. Phase 2 (composite) heel-loading von Mises stress contour, max 1156 MPa.

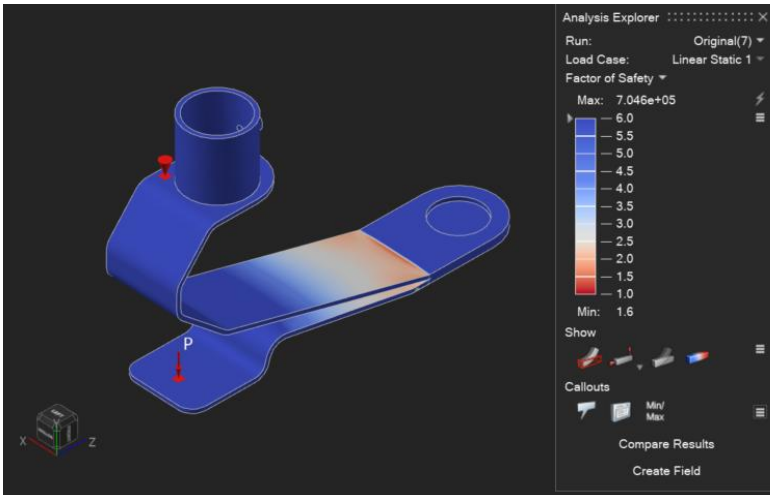

Figure 15. Phase 2 (composite) heel-loading Factor of Safety contour, min 1.6.

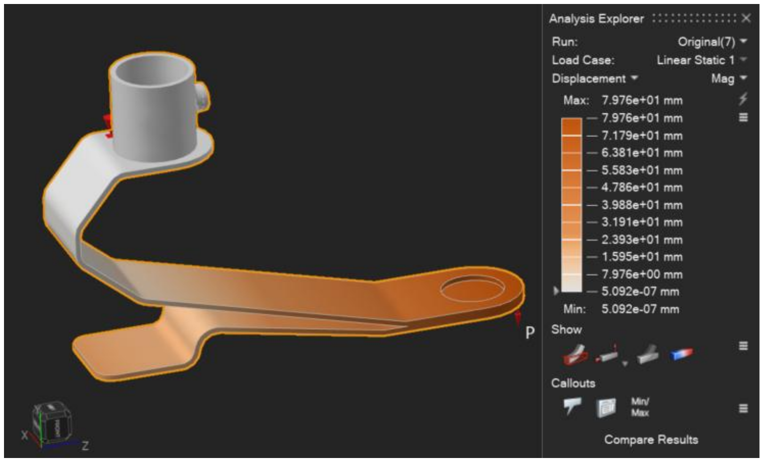

Figure 16. Phase 2 (composite) toe-loading displacement contour at the corrected 0.157 MPa pressure, max 79.76 mm.

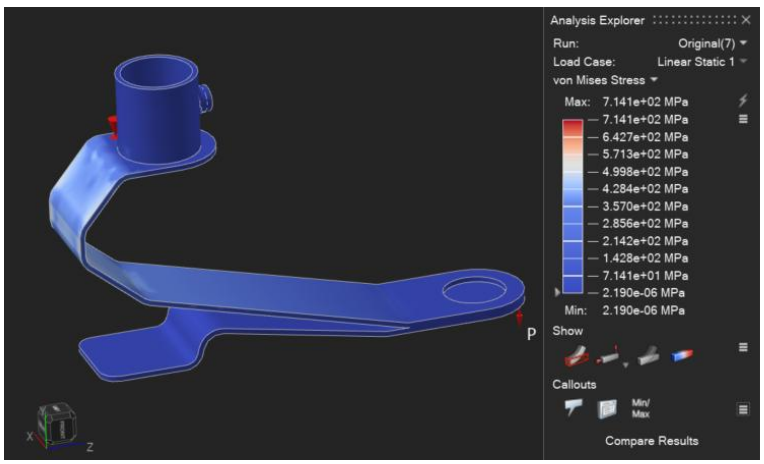

Figure 17. Phase 2 (composite) toe-loading von Mises stress contour at the corrected 0.157 MPa pressure, max 714.1 MPa.

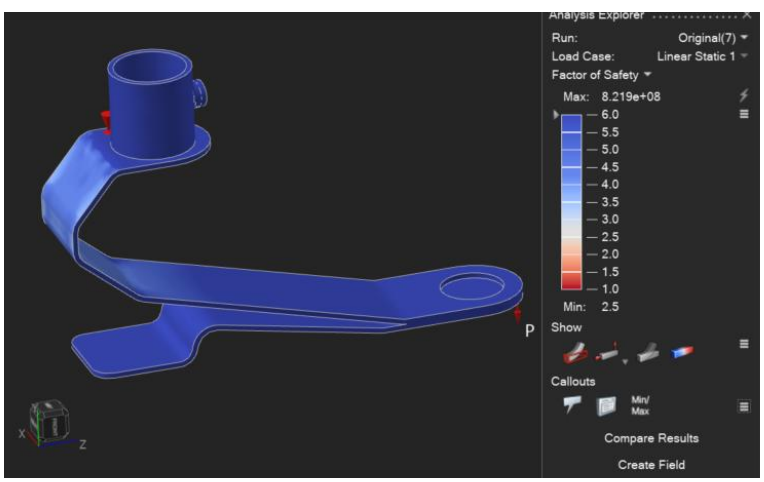

Figure 18. Phase 2 (composite) toe-loading Factor of Safety contour at the corrected 0.157 MPa pressure, min 2.5.

For the composite baseline, the heel-loading case is the governing (more critical) condition, with a minimum FOS of 1.6 compared to 2.5 at the toe.

3.3 Phase 3 — Lattice Site Introduction (Mass Only)

Applying the graded lattice pattern as described in Section 2.7 to the composite produced an initial lattice geometry mass of 0.14 kg, a reduction of 27.8% relative to the composite solid baseline (0.194 kg), corresponding to a relative density of 0.14 / 0.194 ≈ 72.2%. No structural simulation was performed directly on this explicit lattice geometry; it is reported here as a mass and geometric outcome only.

For comparison, the same lattice pattern was applied to the steel solid geometry from Phase 1 for mass-recording purposes only, producing a lattice mass of 0.698 kg and a relative density of 0.698 / 0.968 ≈ 72.1%.

Material	**Solid Mass (kg)**	**Initial Lattice Mass (kg)**	**Relative Density**	**Mass Reduction**
AISI 304 steel (mass check only)	0.968	0.698	72.1%	27.9%
ESAR composite	0.194	0.140	72.2%	27.8%

3.4 Phase 4 — Homogenized Lattice-Zone Structural Analysis (Final Design)

The final lattice-zone configuration was structurally analyzed using the homogenized material properties in Table 2. The final design recorded a total mass of 0.171 kg.

Load Case	**Pressure (MPa)**	**Displacement (mm)**	**Von Mises Stress (MPa)**	**FOS (min)**
Heel	0.285	112.2	1696	1.1
Toe	0.157	110.2	801.3	2.0

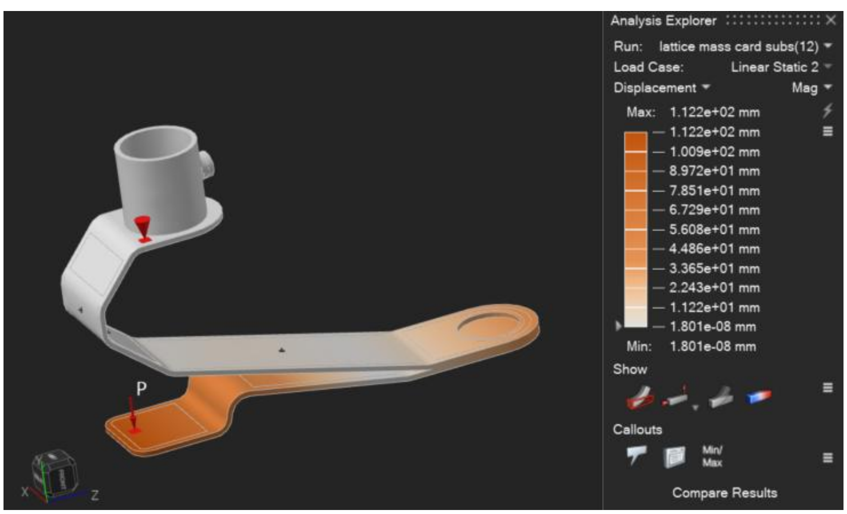

Figure 19. Phase 4 (homogenized lattice) heel-loading displacement (Alwattar & Mian, 2020)*contour, max 112.2 mm.*

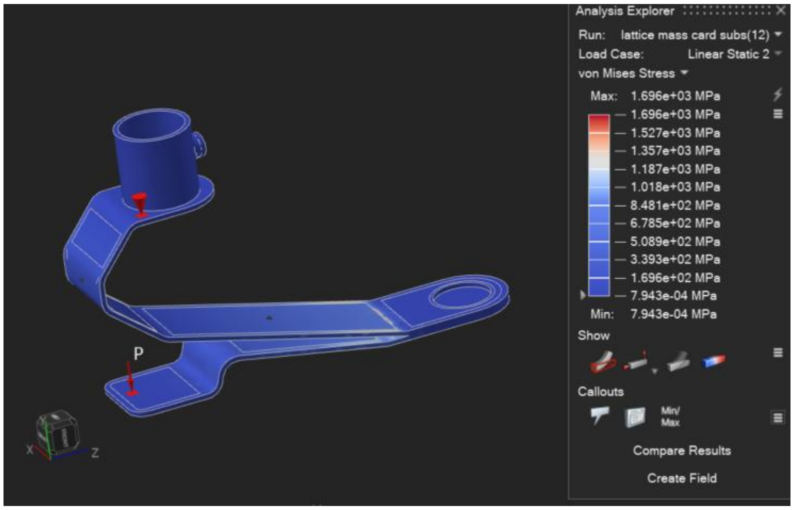

Figure 20. Phase 4 (homogenized lattice) heel-loading von Mises stress contour, max 1696 MPa.

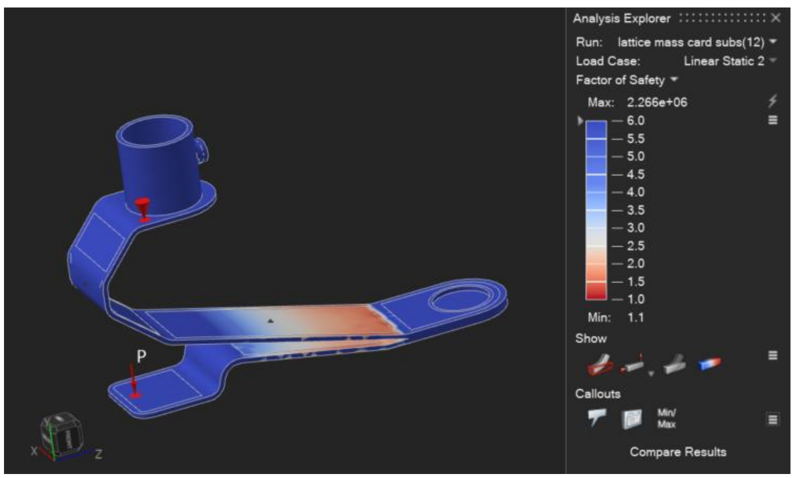

Figure 21. Phase 4 (homogenized lattice) heel-loading Factor of Safety contour, min 1.1.

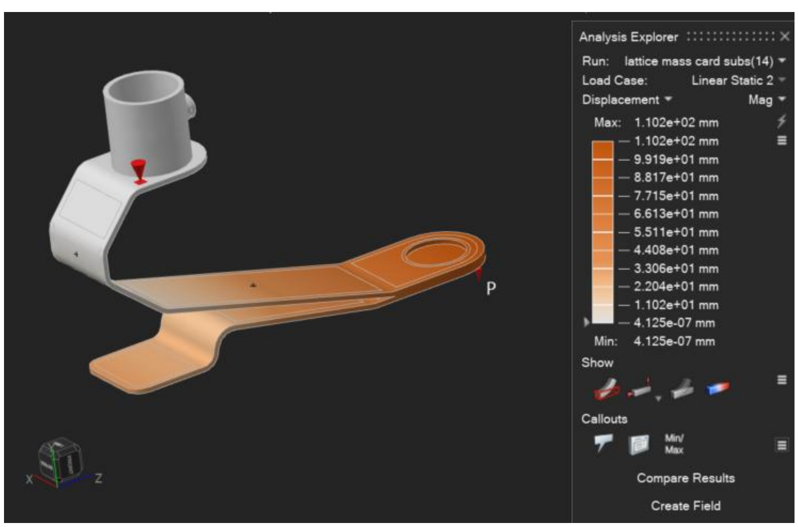

Figure 22. Phase 4 (homogenized lattice) toe-loading displacement contour, max 110.2 mm.

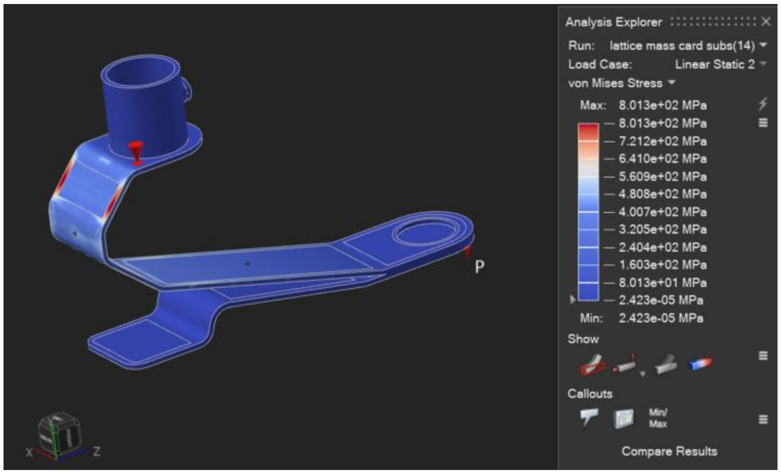

Figure 23. Phase 4 (homogenized lattice) toe-loading von Mises stress contour, max 801.3 MPa.

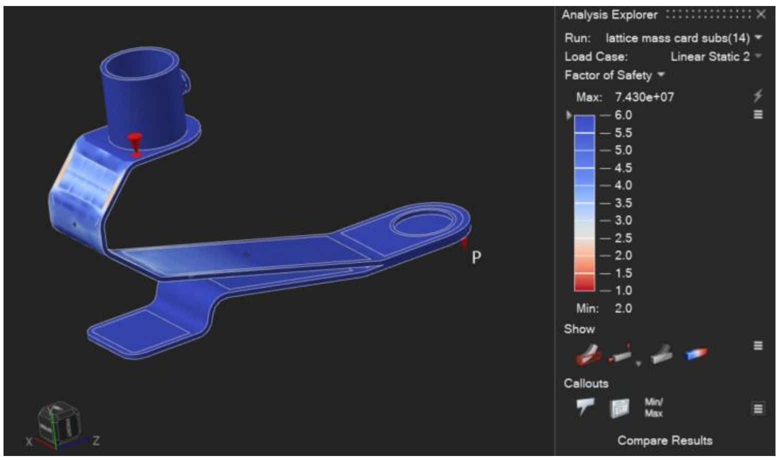

Figure 24. Phase 4 (homogenized lattice) toe-loading Factor of Safety contour, min 2.0.

The heel-loading condition governs the final lattice design, operating at a critical 1.1 Factor of Safety (FoS) near structural failure, compared to a safer 2.0 FoS at the toe. This vulnerability aligns with the Gibson-Ashby scaling relationship (Section 2.8), which dictates that the bending-dominated hex-truss heel (Zone A) loses stiffness faster than the stretch-dominated BCC toe (Zone B) at identical relative densities. It is also consistent with the heel region requiring the earlier cup-area correction outlined in Section 2.9.

3.5 Overall Mass Reduction Across the Study

Combining the material substitution (Phase 1 to Phase 2) and the lattice geometry and structural-correction effects (Phase 2 to Phase 4), the overall mass reduction from the initial steel solid baseline to the final, structurally-evaluated lattice design is:

$$\mathbf{(0.968 - 0.171) / 0.968 \approx 82.3\%}$$

Material substitution alone (Phase 1 to Phase 2, 0.968 → 0.194 kg) accounts for the great majority of the total reduction. The difference between the composite solid mass and the final lattice mass reflects the net effect of introducing lattice geometry into the design. It should therefore not be read as a pure lattice-optimization benefit in isolation but of material substitution as well.

4. Discussion

The four-phase methodology used in this study shows a perspective in light weighting for material selection, lattice geometry, and the analytical method used to evaluate that geometry as a workaround for an approximation perspective for the lattice sites constructed in this ESAR prosthesis.

4.1 Material Effect (Phase 1 vs. Phase 2)

Switching from steel to a composite at a fixed 700 N load turned structural failure (FOS 0.2 – 0.3) into a viable design (FOS 1.6 – 2.5) without altering geometry, proving that material selection is critical for thin, cantilevered ESAR blades.

4.2 Geometric Effect and the Value of Homogenization (Phase 2 vs. Phase 3 vs. Phase 4)

Mass-reduction fractions act as independent geometric properties regardless of base material. The Gibson-Ashby homogenization approach successfully served as a practical design tool, identifying and correcting cup-region weaknesses before finalization.

4.3 Governing Load Case Across Phases

The heel consistently remained the critical structural location across all phases (steel, composite, and final lattice), identifying precisely where future design refinements must focus. The Phase 4 model provides an average stiffness approximation rather than strut-level validation. The minimum FOS of 1.1 acts as an upper-bound estimate because homogenized models cannot capture high local stress concentrations at individual strut junctions.

5. Limitations

- Homogenization & Stress Limits: Phase 4 uses volume-averaged approximations that omit local strut-level stress concentrations, making reported FOS values optimistic upper bounds.
- Analytical & Geometric Constraints: Linear static analysis is strained by large blade displacements (up to 112 mm on a 250 mm blade), and yield stress relied on linear scaling rather than topology-specific modeling.
- Simplified Modeling & Scope: Manual contact boundaries and representative engineering approximations were used instead of continuous physical load paths or test-certified material data, with only a single localized design correction performed.
- Loading & Validation Gaps: Models simulate only a single static condition while omitting dynamic, fatigue, or impact loading, and lack physical prototyping or experimental validation across all phases.

6. Conclusion

A four-phase methodology successfully isolated material and geometric contributions to mass reduction, showing that substituting steel with a composite turned a failing design (FOS 0.2–0.3) into a viable one (FOS 1.6–2.5). Homogenized Lattice Evaluation: Applying Gibson-Ashby scaling to model a graded hex-truss/BCC lattice enabled successful structural evaluation (FOS 1.1 heel, 2.0 toe) and guided critical corrections near the shin-cup interface. The final design achieved an impressive 82.3% overall mass reduction compared to the solid steel baseline, driven primarily by material substitution alongside lattice geometry. Subsequent research must prioritize physical prototyping, direct strut-level simulations, topology-dependent yield scaling, and dynamic gait testing.

References

[1] GrabCAD. Prosthetic Leg (open-source CAD model). Source geometry downloaded, assembled, and cleaned by the author for use in this study from this openly available library; no restricted or proprietary geometry was used.

[2] Alwattar, T. A., & Mian, A. (2020). Developing an Equivalent Solid Material Model for BCC Lattice Cell Structures Involving Vertical and Horizontal Struts. https://www.mdpi.com/2504477X/4/2/74/pdf? (Alwattar & Mian, 2020)version=1592399994

[3] Greer, J. R., & Deshpande, V. S. (2019). Three-dimensional architected materials and structures: Design, fabrication, and mechanical behavior. https://link.springer.com/content/pdf/10.1557/mrs.2019.232.pdf

[4] Hössinger-Kalteis, A., Lackner, M., Major, Z., Karayagiz, F., Nopper, H., & Lück, T. (2024). Design method for individualised 3D printed lattice shoe midsoles. Proceedings of the Institution of Mechanical Engineers, Part L: Journal of Materials: Design and Applications, 239(7), 1422–1432. https://doi.org/10.1177/14644207241291232

[5] Jalali, S. K., Beigrezaee, M. J., Misseroni, D., & Pugno, N. M. (2023). A modified Gibson-Ashby model for functionally graded lattice structures. https://ars.els-cdn.com/content/image/1-s2.0-S0167663623002685-ga1_lrg.jpg

[6] Meyer, G., Brenne, F., Niendorf, T., & Mittelstedt, C. (2020). Influence of the Miniaturisation Effect on the Effective Stiffness of Lattice Structures in Additive Manufacturing. https://www.mdpi.com/2075-4701/10/11/1442/pdf?version=1603969327